Int. J. Heat Mass Transfer. Vol. 31, No. 8, pp. 1627–1634, 1988
Printed in Great Britain

0017–9310/88 $3.00+0.00

Radiative heat transfer in ultra-fine powder insulations

H. S. CHU
Department of Mechanical Engineering, National Chiao Tung University, Hisnchu, Taiwan 30049, Republic of China

and

A. J. STRETTON and C. L. TIEN
Department of Mechanical Engineering, University of California, Berkeley, CA 94720, U.S.A.

(*Received* 31 *August* 1987 *and in final form* 19 *January* 1988)

Abstract—This paper reports the first systematic study of the spectral radiation heat transfer through the ultra-fine powder insulation Aerosil 380. Experimental results are obtained for the spectral extinction coefficient from infra-red transmission measurements and for the effective thermal conductivity using a guarded-hot-plate apparatus. These results are compared and assessed with relevant theoretical calculations. In comparison to total effective conductivity experiments in the temperature range of 320–400 K, radiation heat transfer accounted for approximately 10% of the total heat leakage through the insulation, with the remaining by gaseous conduction. At high temperatures, the radiation contribution is expected to increase sharply, reaching over 50% at about 1000 K.

1. INTRODUCTION

THERMAL insulation has long been a subject of fundamental importance due to its wide application in engineering systems. Several modes of heat transfer in typical porous insulation systems, primarily solid–solid conduction between the particles or fibers, gaseous conduction and convection through the pores of the materials, and radiative transfer through the material, must be minimized in order to attain good thermal performance. Heat transfer through a variety of insulation materials and insulating conditions has been studied extensively in the past. Several review articles on heat transfer in thermal insulation have been reported [1–3].

One of the new concepts which has been advanced recently for thermal insulations involves reducing the gaseous conduction contribution in powdered insulations by utilizing ultra-fine particles with diameters of the order of 100 Å [4, 5]. Indeed, a study of consolidated ultra-fine powder insulations in the form of rigid SiO_2–aerogel tiles for double-pane window applications has been reported [6]. In these insulations, gas conduction can be reduced greatly if the pore size between the solid particles is less than the mean free path of the gas, e.g. about 200 Å for air at 300 K. The resulting effective thermal conductivity through the void spaces will be lower than that of still air, and the high performance of vacuum-assisted insulations can be achieved without evacuating the system. Natural convection in such a system can be neglected due to the small pore size [3]. The solid–solid conduction is also negligible if the solid volume fraction f_v of a material consisting of roughly spherical particles is less than approximately 0.10. The dominant heat transfer modes in ultra-fine powder insulations (UFPI) are gaseous conduction and thermal radiation.

In this study, an SiO_2 ultra-fine powder called Aerosil 380 [7] with particle diameters close to 70 Å has been utilized. The goal is to determine the primary heat transfer mode in this system and to set up models for predicting the effective thermal conductivity of the material as a function of mean temperature and solid volume fraction. Experimentally, the transmission of thermal radiation through the material was measured to deduce the spectral extinction coefficient, and the effective thermal conductivity was measured with a guarded-hot-plate apparatus under various conditions of temperature, solid volume fraction, and internal radiative shields.

2. THEORETICAL CONSIDERATION

2.1. *Radiative transport theory*

For a homogeneous planar system, the radiative heat transfer is one-dimensional and the spectral intensity of radiation I_λ is governed by the equation of transfer, which may be expressed in the form

$$\mu\frac{\partial I_\lambda(y,\mu,\phi)}{\partial y} = -[\sigma_{a\lambda}(T)+\sigma_{s\lambda}(T)]I_\lambda(y,\mu,\phi)$$
$$+\sigma_{a\lambda}(T)I_{b\lambda}(T)+\frac{\sigma_{s\lambda}}{4\pi}\int_{4\pi}\Phi_\lambda(\Omega'\to\Omega)I_\lambda(y,\mu',\phi')\,d\Omega'. \quad (1)$$

NOMENCLATURE

d	particle diameter [m]
f_v	solid particle volume fraction
I	intensity [W m^{-2} sr^{-1}]
k	imaginary part of the complex refractive index
K_{eff}	total effective thermal conductivity [W m^{-1} K^{-1}]
K_g	gas thermal conductivity [W m^{-2}]
K_r	apparent radiant thermal conductivity [W m^{-1} K^{-1}]
L	total thickness of insulation medium
m	complex refractive index, $n-ik$
n	real part of the complex refractive index
N	conduction parameter
q	heat flux [W m^{-2}]
Q	efficiency
T	plate temperature [K]
T_2^*	dimensionless temperature, T_2/T_1
T_m	mean temperature, $(T_1+T_2)/2$ [K]
x	particle size parameter, $\pi d/\lambda$
y	slab coordinate [m].

Greek symbols

ε	plate emissivity
θ	polar angle of the plane parallel slab [rad]
λ	wavelength [m]
μ	$\cos\theta$
σ	Stefan–Boltzmann constant, 5.678×10^{-8} W m^{-2} K^{-4}
σ_a	absorption coefficient [m^{-1}]
σ_e	extinction coefficient [m^{-1}]
$\bar{\sigma}_e$	Rosseland mean extinction coefficient [m^{-1}]
σ_s	scattering coefficient [m^{-1}]
ϕ	azimuthal angle of the slab [rad]
Φ_λ	scattering phase function
Ω	solid angle [sr].

Subscripts

a	absorption
b	blackbody
D	dependent scattering
e	extinction
g	gas
I	independent scattering
m	mean
r	radiation
s	scattering
λ	wavelength
1	hot plate
2	cold plate.

In equation (1), $\mu=\cos\theta$, $\sigma_{a\lambda}(T)$ and $\sigma_{s\lambda}(T)$ are the absorption coefficient and the scattering coefficient, respectively, y the coordinate, θ the polar angle, ϕ the azimuthal angle, $I_{b\lambda}(T)$ the Planck blackbody intensity function, T the temperature, Φ the scattering phase function, Ω the solid angle, and subscript λ and superscript $'$ denote spectral quantity and in-coming, respectively. It is implicitly assumed in equation (1) that the participating medium is isotropic otherwise $\sigma_{a\lambda}(T)$ and $\sigma_{s\lambda}(T)$ would also be a function of direction. For the case of a cold homogeneous medium, under the influence of a relatively strong but unidirectional beam of radiant energy, the emission terms and in-scattering terms are negligible and the solution is given by Beer's law

$$I_\lambda(y)=I_\lambda(0)\exp(-\sigma_{e\lambda}y) \tag{2}$$

where $\sigma_{e\lambda}=(\sigma_{a\lambda}+\sigma_{s\lambda})$ is the extinction coefficient. For the case of an optically thick medium where radiation can be treated as a diffusion process, the radiant heat transfer is simply [8]

$$q_r=\frac{\sigma(T_1^4-T_2^4)}{\frac{3}{4}\bar{\sigma}_e L+\frac{1}{\varepsilon_1}+\frac{1}{\varepsilon_2}-1}=-K_r\left(\frac{T_2-T_1}{L}\right) \tag{3}$$

where K_r is the apparent radiant thermal conductivity, the boundaries have temperatures T_1, T_2 and emissivities ε_1, ε_2, respectively, and L is the distance between the boundaries. Note that the Rosseland mean extinction coefficient $\bar{\sigma}_e$ [8] for an optically thick medium is used instead of the spectral coefficient $\sigma_{e\lambda}$. For moderate temperature differences less than 200 K [9], the apparent radiant thermal conductivity can be described by

$$K_r=\frac{4\sigma T_m^3 L}{\frac{3}{4}\bar{\sigma}_e L+\frac{1}{\varepsilon_1}+\frac{1}{\varepsilon_2}-1} \tag{4}$$

where T_m is the arithmetic mean of the boundary temperatures.

2.2. *Radiative properties*

The radiative property of the powders, required for heat transfer calculations with the diffusion approximation method, is the extinction coefficient σ_e, or alternatively, the absorption coefficient σ_a combined with the scattering coefficient σ_s. By assuming independent scattering, these properties can be derived and computed by solving the Maxwell equations with appropriate boundary conditions and using measured optical constants. Rayleigh scattering theory can be used to calculate the absorption and scattering coefficients for UFPI for extremely small values of

the particle size parameter ($x = \pi d/\lambda \ll 1$) [10]. The extinction coefficient for uniform-size powders with diameter d is [11]

$$\sigma_{c\lambda} = \frac{3f_v}{2d}[Q_{a\lambda} + Q_{s\lambda}] \tag{5}$$

where $Q_{a\lambda}$ and $Q_{s\lambda}$ are the absorption and scattering efficiencies, respectively. If the radiation interaction with each particle can be considered independently of its neighbors, then using Rayleigh scattering theory for a single spherical particle gives

$$Q_{a\lambda,I} = -4x \operatorname{Im}\left\{\frac{m^2-1}{m^2+2}\right\} \tag{6}$$

$$Q_{s\lambda,I} = \frac{8}{3}x^4\left|\frac{m^2-1}{m^2+2}\right|^2 \tag{7}$$

where $m = n - ik$ is the complex index of refraction, and the parameters n, k, x are all strong functions of wavelength.

The assumption of independent scattering and absorption by the particles may not be valid for UFPI [9, 12], in which case the dependent coefficients can be estimated from the independent coefficients. Making use of the Percus–Yevick distribution [13, 14] in the limit of x approaching zero, the ratio of the dependent scattering efficiency $Q_{s\lambda,D}$ to the independent case efficiency $Q_{s\lambda,I}$ is given by

$$\frac{Q_{s\lambda,D}}{Q_{s\lambda,I}} = \frac{(1-f_v)^4}{(1+2f_v)^2}. \tag{8}$$

Kunitomo *et al.* [15] experimentally showed the trend of a decrease in the scattering efficiency with increasing f_v, and also indicated an increasing trend in the absorption efficiency such that

$$\frac{Q_{a\lambda,I}}{Q_{a\lambda,D}} \approx \frac{Q_{s\lambda,D}}{Q_{s\lambda,I}} = \frac{(1-f_v)^4}{(1+2f_v)^2}. \tag{9}$$

This trend is well supported for $f_v < 0.1$ by the theoretical results of ref. [16].

3. EXPERIMENTS

Since the primary function of thermal insulation is to reduce heat flow through insulation, it is important to realize the various heat transfer processes responsible for this heat flow. In this study, the total effective thermal conductivity was measured. In order to realize the contribution of radiative heat transfer in UFPI, the infra-red transmission measurements were carried out. Based on these experimental data, the radiative heat transfer in UFPI can be obtained.

3.1. *Description of the apparatus*

The infra-red transmission apparatus consists of three basic components: the source unit and associated optics, a spectral radiation detector matched to the source, and the sample cell. A schematic diagram illustrating the basic system and the details of the sample cell is provided in Fig. 1. A variety of source and detector combinations were utilized to access as much of the infra-red electromagnetic spectrum as possible.

The test cell consisted simply of a layer of Aerosil 380 sandwiched between two infra-red windows. The windows were made of pure crystalline sodium chloride, 25 mm in diameter and 4 mm thick, polished to optical flatness and capable of transmitting approximately 90% of the incident radiant energy over the entire measured spectral region. The distance between the windows was preset by means of three spacer shims, each approximately 1 mm square and exactly equal in thickness, with a variety of thicknesses available to provide different optical path lengths. The perimeter of the test cell volume was bounded by a rubber retainer 1.5 mm thick, which made it possible to enclose a measured mass of the powder (0.5–8 mg) within a known volume to calculate f_v. The action of screwing down the retaining ring on the sample holder to fix the windows into position during the test cell assembly tended to also turn the upper window and thus spread the powder evenly throughout the test cell volume to produce a homogeneous layer consistent with the theoretical analysis. However, this method of sample preparation was limited to a range of f_v between 0.025 and 0.06 for Aerosil 380, otherwise significant areas of inhomogeneous density were observed within the test cell cross-section.

In the near infra-red range, three different lasers were used to obtain data for the wavelengths 0.532, 0.6328, and 1.053 μm. Each laser produced a circularly polarized beam 1 mm in diameter, which was expanded and re-collimated through a pair of convex lenses of focal lengths 5.72 and 50 mm, and then passed through an iris diaphragm to reduce the diameter of the incident beam. The rationale for expanding and then cutting down the beam diameter was to minimize two-dimensional effects due to the Gaussian radial distribution of the intensity of the laser beam. A diameter of at least five times the powder thickness was maintained in order to approximate a plane-parallel one-dimensional geometry as assumed in the theoretical analysis. After passing through the test cell, the beam was collected by a lens tube assembly consisting of a field stop, an aperture stop, and an achromatic lens which focused the beam onto the photocathode surface of a photomultiplier tube detector. The aperture stop defined the solid angle of the cone of the detected beam and the field stop limited the detector's field of view of the total beam.

In the infra-red range from 0.8 to 16 μm, two different experimental facilities were used. The source of the first apparatus was a silicon carbide rod electrically heated at approximately 1100 K, combined with a set of first-surface mirrors to produce a parallel beam to transfer the test cell and also to focus the transmitted beam from the test cell on the detector entrance, which was a Perkin–Elmer Model 99 prism monochromator capable of measuring in the range of 1.7–16 μm. The

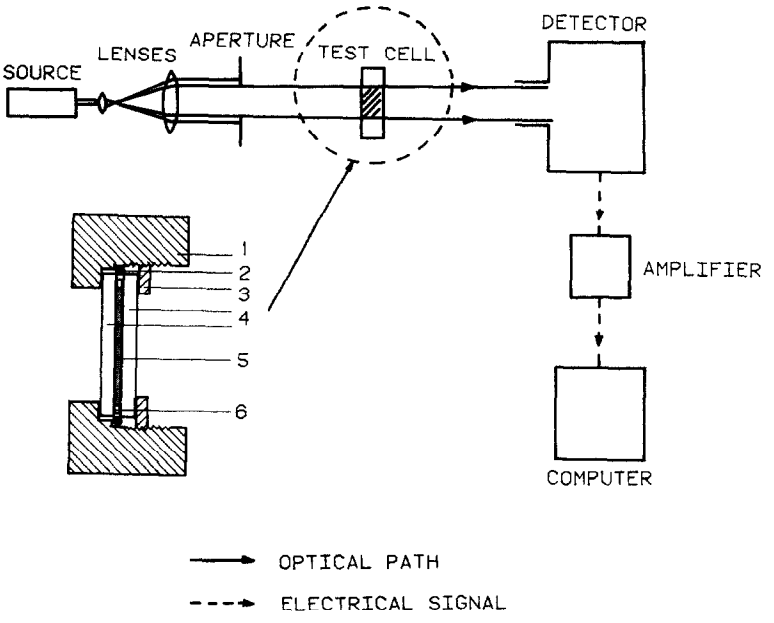

FIG. 1. Schematic diagram of the experimental apparatus for measuring the transmission of radiation: 1, aluminum holder; 2, rubber retaining ring; 3, plastic holding ring; 4, infra-red windows; 5, powder insulation; and 6, spacing shim.

second apparatus was a Perkin–Elmer Model Lambda 9 spectrophotometer with a built-in source and detector covering the range 0.8–3.2 μm. The spectral transmission data from both of the infra-red detectors were collected by dedicated data acquisition systems and stored in computer files for later processing.

The guarded-hot-plate apparatus for measuring the total effective thermal conductivity was constructed of two layers of Aerosil 380 clamped between three isothermal copper plates with the center plate heated and the outer plates cooled. The center hot plate consisted of a central metering area surrounded by an independently heated guard perimeter area to prevent edge effects. The details of the apparatus are described in a previous paper dealing with fibrous insulation [17]. A regulated power supply was used for the heater circuit of the metered section of the apparatus to insure a constant heat input regardless of variations in the line voltage. Fourteen copper–constantan thermocouples were installed in shallow grooves machined into the surfaces facing the UFPI layers, in order to check the isothermal criteria for the hot-plate surface temperature. Each of the Aerosil powder layers was contained within a supportive testing container molded from 5 mm thick Fiber-frax insulation material. The reason for fabricating a special container for the test material is that Aerosil 380 UFPI behaves like a flowing powder for $f_v < 0.03$, but becomes a very brittle compacted solid for $0.03 < f_v < 0.1$.

3.2. *Experimental procedure*

Two different sample cells were made for the transmission measurements, one with heat treatment to reduce moisture content, and one without. The powder with treatment was heated to 1000 K for 1 h and then kept at 500 K for 24 h under vacuum conditions. The thickness of each sample cell was 0.0635 mm for the untreated powder and 0.127 mm for powder with treatment. After the treated powder was taken out from the furnace, the sample cell was made as quickly as possible to limit the re-absorption of atmospheric moisture by the powder. A reference cell was made for each sample cell in exactly the same manner as the sample cell, except that no powder was placed between the two infra-red windows. The infra-red transmittance of the powder was determined by simply taking the ratio of the spectral signals which passed through the sample cell and the reference cell, respectively.

For each run with the guarded-hot-plate apparatus, the hot and cold plates were maintained at constant temperature to achieve steady-state conditions. Due to the temperature limitations of at least 5 K above the ambient for the cold bath, the cold plate was set at 308 K and kept at this value throughout all the experiments. The hot plate was run with different temperatures ranging from 330 to 480 K to investigate the temperature dependence of the effective thermal conductivity of the Aerosil powder. The temperature difference between the hot plate and the surrounding guard plate was kept below 0.1 K with the assistance of a regulator. The average plate temperature difference $\Delta T = (T_1 - T_2)$ was recorded every hour, and steady state was considered to be achieved when three successive sets of observations gave temperatures differing by less than 0.5 K (approximately 15 h). The electrical power input supplied to the hot plate was

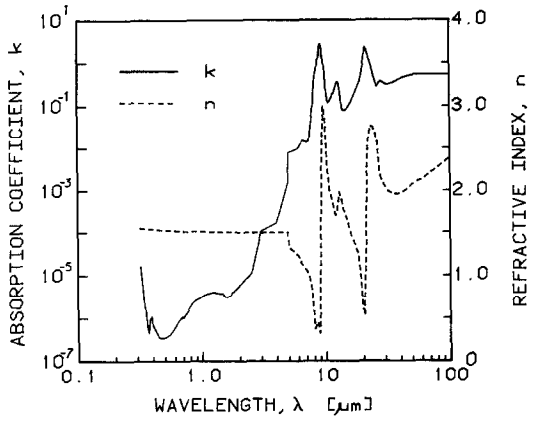

FIG. 2. The complex refractive index components for Aerosil 380.

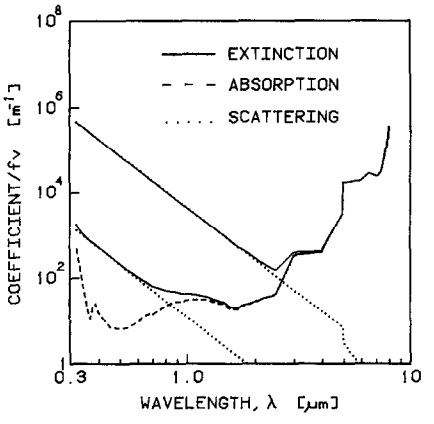

FIG. 3. The scattering, absorption and extinction properties of Aerosil 380 at two different size distributions.

recorded once equilibrium was established, in order to determine the total heat flow through the two layers of insulation. After obtaining several data points, the samples were then removed from the apparatus so that new samples could be inserted. These new samples contained either one or two radiation shields inside them so as to further examine the heat transfer properties of Aerosil 380.

4. RESULTS AND DISCUSSION

4.1. *Calculated radiative properties*

The information required to calculate the radiative properties of UFPI are the complex refractive index of the bulk material making up the particles, the solid volume fraction f_v, and the characteristic particle size d.

Figure 2 shows the n and k values for Aerosil which were used for calculation. The data in the wavelength range 0.32–4.95 and 27.55–124 μm were taken from tabulated values by Hsieh and Su [18], in the range 5.0–6.5 μm from a report by Lang and Wolfe [19], and in the range 7.0–26.0 μm from a paper by Champetier and Friese [20]. The figure shows a strong absorption band centered at 9 μm and a companion strong refractive index peak near 10 μm. A second absorption peak which is also strong but broader occurs at 22 μm and the corresponding refractive index peak is found at 24 μm.

The complex index of refraction values have been used along with the particle size parameter to theoretically calculate the radiation properties of the powder at two different size distributions, 70 and 500 Å. In Fig. 3, the parameter σ_e/f_v is comparatively large in the long wavelength region because the imaginary component of the complex refractive index, which accounts for radiative absorption, is also large in this region. The scattering contribution is negligible at long wavelengths and dominant at short wavelengths because the scattering coefficient is proportional to the fourth power of the size parameter x. The two curves plotted in Fig. 3 demonstrate that for $d = 70$ Å, scattering becomes dominant at $\lambda < 0.5$ μm, but for $d = 500$ Å, scattering is dominant over a larger range extending to 2.0 μm. Comparing the two extinction curves, one can also see that the σ_e/f_v curve for $d = 500$ Å is much higher than that of $d = 70$ Å due to the effect of scattering when $\lambda < 2$ μm. This trend indicates that if the particles agglomerate into large secondary particles, the extinction coefficient will also be large in the lower wavelength regions.

4.2. *Experimental extinction coefficient*

Transmission measurements were made in the wavelength range 0.532–16 μm, from which the extinction coefficient σ_e was calculated according to Beer's law in equation (2). In Fig. 4, experimental data have been presented in a comparison with the theoretical results. The dotted line represents independent scattering and absorption with the particle diameter set to 70 Å, while the solid line is the distribution for dependent scattering and absorption. The dashed line illustrates the results published by McElroy *et al.* [21], for which an experimental correlation was used to modify the independent scattering to dependent scattering. In the longer wavelength regions, it can be seen that the results of McElroy *et al.* correspond with the present theoretical independent calculations of the extinction coefficient. The discrepancy between the predictions of McElroy *et al.* and the present results in the low-wavelength region is due to the different values used by each group for the optical properties of silicon dioxide.

The comparison between the experimental data and the theoretical results demonstrates that for wavelengths greater than 7 μm, the experimental data agree with the theoretical calculations quite well due to the strong absorption of silicon dioxide. For $\lambda < 6$ μm, one finds that the experimental data for Aerosil 380 are much higher than the theoretical results, probably due to the adsorption of moisture by the powder causing the primary particles to agglomerate into large secondary particles or chains of particles. The scattering coefficient increases very quickly in this case,

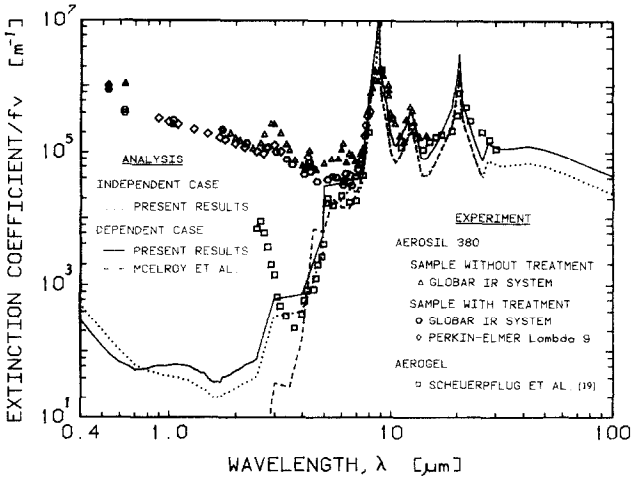

FIG. 4. The spectral extinction coefficient for Aerosil 380. The experimental data was deduced according to Beer's law from transmission measurements.

giving a very high extinction coefficient in the low-wavelength region.

Since the scattering behavior involved several factors beyond the scope of the present investigation, two sets of transmission experiments were carried out in the low-wavelength region to provide additional clues. One set involved powder without any special preparation, while the other was heat treated to reduce the free-moisture content, as opposed to the adsorbed surface moisture which requires more elaborate procedures. In the data for the sample without heat treatment, it can be seen that the absorption bands at $\lambda = 2.7$ and 6.3 μm are reduced in the spectra of the heat-treated samples.

Comparisons of σ_e/f_v between the Aerosil 380 and aerogel [6] materials have also been conducted. The data from both materials are close to the theoretical results for $\lambda > 7$ μm, but below this wavelength range they show a large discrepancy. This phenomenon can be attributed to the difference in structure between the two materials, by which aerogel resists moisture absorption and agglomeration into larger particles due to its lattice construction. This feature also helps to explain why the extinction coefficient of aerogel almost coincides with the theoretical curve in the region of 3–7 μm, while the Aerosil is several orders of magnitude higher in this region. In the long-wavelength region, the experimental data tend towards the dependent theoretical case, implying that dependent absorption may be important in radiation heat transfer through Aerosil powder insulation.

The experimental data show a small peak at $\lambda = 4.3$ μm, which would seem to indicate that the Aerosil powder has traces of CO_2 in the spectrum. This band is believed to be a spurious anomaly caused by CO_2 absorption in the prism of the monochromator detector, which was unable to provide consistent zero checks in the wavelength neighborhood of this band.

4.3. *Effective thermal conductivity*

The effective thermal conductivity was calculated according to Fourier's law of heat conduction from the experimentally determined data of the guarded-hot-plate apparatus. The range of experimental conditions investigated was 320–395 K for the mean temperature and 0.027 and 0.055 for the solid volume fraction f_v. The mean extinction coefficient was deduced from the transmission experiments where σ_e/f_v ranged from approximately 1.0×10^5 at 300 K to 7.5×10^4 at 400 K. The radiant thermal conductivity at different mean temperatures was calculated with equation (4), which was derived by the diffusion-approximation method. The radiant thermal conductivity at the various mean temperatures was also calculated by a more sophisticated combined conduction and radiation model derived in ref. [22]

$$q = \frac{[3N(1-T_2^*)+(1-T_2^{*4})]\sigma T_1^4}{\frac{3}{4}\bar{\sigma}_e L + \frac{\frac{3}{8}+\frac{1}{3}(1-\varepsilon_1)}{N+\frac{2}{3}\varepsilon_1} + \frac{\frac{3}{8}+\frac{1}{3}(1-\varepsilon_2)}{(N/T_2^{*3})+\frac{2}{3}\varepsilon_2}} \quad (10)$$

where $N = k_g\bar{\sigma}_e/(4\sigma T_1^3)$ is a parameter relating the thermal conductivity of the gas to the effective radiative thermal conductivity, $T_2^* = T_2/T_1$ and subscripts 1 and 2 refer to the hot and cold surfaces, respectively. The comparison of the analysis by the two methods is shown in Figs. 5 and 6 for each of the solid volume fractions investigated. The effective gas conductivity K_g was obtained simply by subtracting the radiative thermal conductivity K_r from the total effective conductivity K_{eff}. The radiant thermal conductivity calculated by the combined model compared to that of the simple diffusion model is slightly greater, differing by only 2.3–7.3% at mean temperatures ranging from 320 to 400 K, respectively. The difference between the two models referred to the total effective thermal conductivity is less than 1%, indicating that within this low range of mean temperatures, the diffusion method is a good approximation to calculate the radiant contribution to the effective thermal conductivity. However, the difference of radiant thermal conductivity between the models increases with the mean temperature such that the accuracy of the simple diffusion-approximation method is questionable at

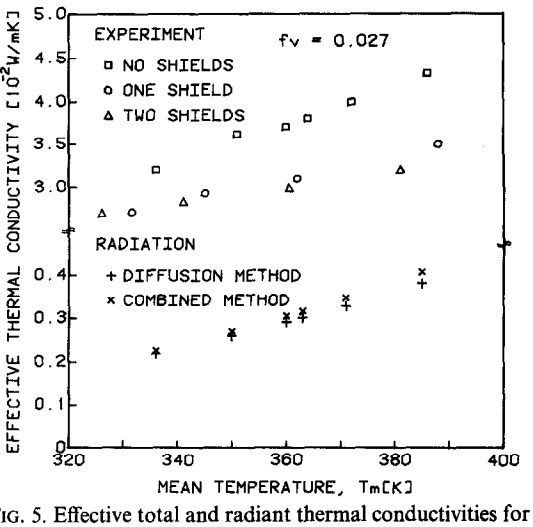

FIG. 5. Effective total and radiant thermal conductivities for the cases of no shield, one shield and two shields at a solid volume fraction of 0.027.

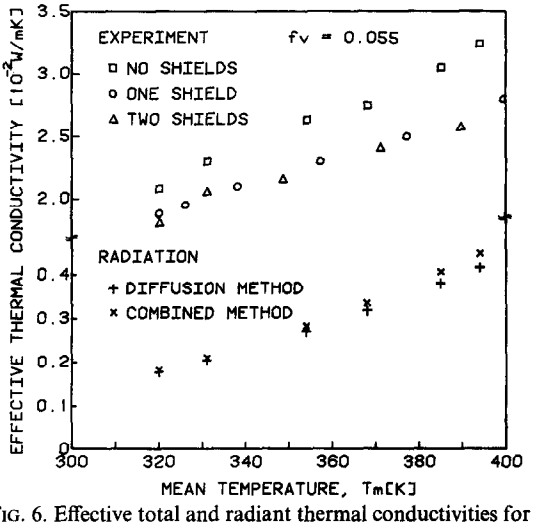

FIG. 6. Effective total and radiant thermal conductivities for the cases of no shield, one shield and two shields at a solid volume fraction of 0.055.

high temperatures. The conduction–radiation analysis gives that the gas conductivity K_g is 92% of the total effective conductivity K_{eff} at $T_m = 320$ K and is 88% of K_{eff} at $T_m = 394$ K. The gas-conduction contribution is dominant at temperatures near room temperature, and radiation contributes less than 12% to the total effective thermal conductivity of Aerosil 380 below 400 K. The trend of the radiative thermal conductivity displays a cubic relationship with mean temperature, as expected by the close correspondence to the diffusion model, which emphasizes that radiation heat transfer must be considered at high temperatures. A simple estimate based on linear extrapolation of the total effective conductivity to high temperatures shows that the radiation contribution will reach over 50% at about 1000 K.

5. CONCLUSIONS

The radiative heat transfer in a typical ultra-fine powder insulation has been investigated both theoretically and experimentally and compared to the total effective thermal conductivity measured by a guarded-hot-plate experiment. The diffusion-approximation method is an excellent approximation for calculating the radiant thermal conductivity for Aerosil 380 at temperatures ranging from 300 to 400 K. The predictions of the spectral extinction coefficient from available data on the optical properties of silicon dioxide are good in the absorption-dominated regime above 8 μm, but are low by a factor of 1000 in the scattering-dominated regime below 6 μm. In the limited temperature range of the experiments conducted, radiation accounted for only 8.8–12.5% of the total heat leakage through the UFPI insulation, thus the dominant heat leakage through Aerosil 380 at moderate temperatures is due to gas conduction. The radiant contribution to the total heat leakage increases as the third power of the mean temperature, indicating that it is important in higher temperature applications where reflective shields can be used to significantly improve the performance of the insulator. The Aerosil particles demonstrate a strong tendency to agglomerate into secondary particles with large effective diameters, which significantly affect both the gas conduction and the radiation properties of the material. The effective total thermal conductivity of the ultra-fine powder could be lowered by one order of magnitude if the agglomeration behavior is prevented, which would make it comparable with the conductivity of vacuum-assisted insulations.

REFERENCES

1. P. E. Glaser *et al.*, Thermal insulation systems, NASA SP-5027 (1967).
2. C. L. Tien and G. R. Cunnington, Cryogenic insulation heat transfer. In *Advances in Heat Transfer*, Vol. 9, pp. 349–417. Academic Press, New York (1973).
3. R. P. Tye (Editor), *Thermal Transmission Measurements of Insulation*. ASTM STP-660 (1978).
4. C. L. Tien and K. Y. Wang, Thermal insulation heat transfer, *Special Issue for the U.S.–China Binational Heat Transfer Workshop, J. Engng Thermophys.* 1–11 (1984).
5. D. W. Yarbrough, T. W. Tong and D. L. McElroy, Use of fine powders for high thermal resistance, *High Temp. Sci.* **19**, 213–225 (1985).
6. P. Scheuerpflug, R. Caps, D. Buttner and J. Fricke, Apparent thermal conductivity of evacuated SiO_2–aerogel tiles under variation of radiative boundary conditions, *Int. J. Heat Mass Transfer* **28**, 2299–2306 (1985).
7. R. Bode, H. Ferch and H. Fratzscher, Basic characteristics and applications of aerosil, Technical Bulletin No. 11, Degussa Inc., Frankfurt, Federal Republic of Germany (1967).
8. R. Siegel and J. R. Howell, *Thermal Radiation Heat Transfer*, 2nd Edn, pp. 473–474, 637–638. Hemisphere, New York (1981).
9. C. L. Tien and B. L. Drolen, Thermal radiation in particulate media with dependent and independent scat-

tering. In *Annual Review of Numerical Fluid Mechanics and Heat Transfer*, Vol. 1, pp. 1–32. Hemisphere, New York (1986).
10. H. C. van de Hulst, *Light Scattering by Small Particles*. Dover, New York (1981).
11. K. Y. Wang and C. L. Tien, Radiative heat transfer through opacified fibers and powders, *J. Quant. Spectrosc. Radiat. Transfer* **30**, 213–223 (1983).
12. M. Q. Brewster and C. L. Tien, Radiative transfer in packed/fluidized beds: dependent versus independent scattering, *J. Heat Transfer* **104**, 573–579 (1982).
13. L. Tsang, J. A. Kong and T. Habashy, Multiple scattering of acoustic waves by random distribution of discrete spherical scatterers with the quasicrystalline and Percus–Yevick approximation, *J. Acoust. Soc. Am.* **71**, 552–558 (1982).
14. V. Twersky, Acoustic bulk parameters in distributions of pair-correlated scatterers, *J. Acoust. Soc. Am.* **64**, 1710–1719 (1978).
15. T. Kunitomo, Y. Tsuboi and H. M. Shafey, Dependent scattering and dependent absorption of light in a fine-particle dispersed medium, *Bull. J.S.M.E.* **28**, 854–859 (1985).
16. S. Kumar and C. L. Tien, Dependent scattering and absorption of radiation by small particles. In *Fundamentals and Applications of Radiation Heat Transfer*, 24th National Heat Transfer Conference, Pittsburgh, Pennsylvania, 9–12 August 1987 (Edited by A. M. Smith and T. F. Smith), ASME HTD-Vol. 72, pp. 1–7 (1987).
17. T. W. Tong, Q. S. Yang and C. L. Tien, Radiative heat transfer in fibrous insulations—Part II: experimental study, *J. Heat Transfer* **105**, 76–81 (1983).
18. C. K. Hsieh and K. C. Su, Thermal radiative properties of glass from 0.32 to 200 μm, *Solar Energy* **22**, 37–43 (1979).
19. M. L. Lang and W. L. Wolfe, Optical constants of fused silica and sapphire from 0.3 to 25 μm, *Appl. Optics* **22**, 1267–1268 (1983).
20. R. J. Champetier and G. J. Friese, Use of polished fused silica to standardize directional polarized emittance and reflectance measurements in the infrared, SAMSO-TR-202, The Aerospace Corporation, El Segundo, California (1974).
21. D. L. McElroy, D. W. Yarbrough, G. L. Copeland, F. J. Weaver, R. S. Graves, T. W. Tong and H. A. Fine, Development of advanced thermal insulation for appliances, L/CON-159, Oakridge National Laboratory, Oakridge, Tennessee (1984).
22. L. S. Wang and C. L. Tien, A study of various limits in radiation heat transfer problems, *Int. J. Heat Mass Transfer* **10**, 1327–1338 (1967).

TRANSFERT DE CHALEUR RADIATIF DANS DES POUDRES ULTRA-FINES POUR ISOLATION

Résumé—On décrit la première étude systématique du rayonnement thermique à travers une poudre ultra-fine Aerosil 380 pour isolation. Des résultats expérimentaux sont obtenus pour le coefficient spectral d'extinction à partir des mesures de transmission par infrarouge et pour la conductivité thermique effective en utilisant un appareil à plaque chaude gardée. Ces résultats sont comparés et confirmés par des calculs théoriques. En comparaison avec les expériences de conductivité effective totale, dans le domaine de température entre 320 et 400 K, le rayonnement thermique compte pour 10% du flux total à travers l'isolant. Aux températures élevées la contribution du rayonnement augmente fortement pour atteindre plus de 50% vers 1000 K environ.

WÄRMEÜBERTRAGUNG DURCH STRAHLUNG IN WÄRMEDÄMMUNGEN AUS ULTRA-FEINEM PULVER

Zusammenfassung—In dieser Arbeit wird über die erste systematische Untersuchung der spektralen Strahlungswärmeübertragung durch die ultra-feine pulverförmige Wärmedämmung "Aerosil 380" hindurch berichtet. Experimentelle Ergebnisse wurden für den spektralen Extinktionskoeffizienten aus Messungen der infraroten Transmission und für die effektive Wärmeleitfähigkeit durch Verwendung eines Platten-Apparats erzielt. Diese Ergebnisse werden mit theoretischen Berechnungen verglichen und bewertet. Im Vergleich zu den Untersuchungen der effektiven Wärmeleitfähigkeit im Temperaturbereich von 320 bis 400 K ist die Wärmeübertragung durch Strahlung zu annähernd 10% für den gesamten Wärmeverlust durch die Wärmedämmung verantwortlich, wobei der Rest durch Wärmeleitung der Gase bewirkt wird. Bei hohen Temperaturen wird vermutet, daß der Beitrag der Strahlung stark anwächst und bei ungefähr 1000 K über 50% erreicht.

РАДИАЦИОННЫЙ ТЕПЛОПЕРЕНОС В ИЗОЛЯЦИОННЫХ МАТЕРИАЛАХ ИЗ УЛЬТРАДИСПЕРСНЫХ ПОРОШКОВ

Аннотация—Представлены результаты первого систематического изучения спектральных характеристик радиационного теплопереноса через изолирующий материал из ультрадсперсного порошка Аэросил-380. Экспериментальные результаты для спектрального коэффициента затухания получены с помощью измерений передачи инфракрасного излучения, а для эффективной теплопроводности—с использованием установки с тепловым экраном. Результаты сравниваются с соответствующими теоретическими расчетами. По сравнению с экспериментами по определению полной эффективной теплопроводности для диапазона температур 320–400 K, радиационный теплоперенос учитывает примерно 10% общей утечки тепла через изоляцию, причем оставшееся тепло передается газом. При высоких температурах ожидается резкое увеличение излучения, достигающее примерно 50% при $t = 1000$ K.